Journal of Theoretical Biology 335 (2013) 185–197

Contents lists available at SciVerse ScienceDirect

Journal of Theoretical Biology

journal homepage: www.elsevier.com/locate/yjtbi

Mineralization-driven bone tissue evolution follows from fluid-to-solid phase transformations in closed thermodynamic systems

Claire Morin, Christian Hellmich *

Institute for Mechanics of Materials and Structures, Vienna University of Technology, Karlsplatz 13, 1040 Vienna, Austria

HIGHLIGHTS

- Extracellular bone tissue mineralizes under closed thermodynamic conditions.
- Fibrillar and extrafibrillar masses are preserved during mineralization.
- Precipitation of mineral ions leads to volume shrinkage of mineralizing bone tissue.
- Neutron diffraction data provide experimental access to fibrillar volume shrinkage.

ARTICLE INFO

Article history:
Received 5 February 2013
Received in revised form
10 June 2013
Accepted 12 June 2013
Available online 28 June 2013

Keywords:
Neutron diffraction
Mass conservation
Shrinkage
Hydroxyapatite precipitation
Fibrils

ABSTRACT

The fundamental mechanisms that govern bone mineralization have been fairly well evidenced by means of experimental research. However, rules for the evolution of the volume and composition of the bone tissue compartments (such as the mineralized collagen fibrils and the extrafibrillar space in between) have not been provided yet. As an original contribution to this open question, we here test whether mineralizing bone tissue can be represented as a thermodynamically closed system, where crystals precipitate from an ionic solution, while the masses of the fibrillar and extrafibrillar bone tissue compartments are preserved. When translating, based on various experimental and theoretical findings, this mass conservation proposition into diffraction–mass density relations, the latter are remarkably well confirmed by independent experimental data from various sources. Resulting shrinkage and composition rules are deemed beneficial for further progress in bone materials science and biomedical engineering.

1. Introduction

Bone mineralization is a very complicated process where several microns-sized osteoblastic cells release, through budding from their membranes, so-called matrix vesicles (sized tens of nanometers) into the extracellular space (Anderson et al., 2005; Anderson and Reynolds, 1973; Wiesmann et al., 2004). These vesicles carry all molecular components for triggering a multistage process, binding mainly calcium to phosphate ions, which finally results in the precipitation of hydroxyapatite in the form of nanocrystals. The latter then penetrate the vesicles' membranes, and continue to grow into the ("extra-vesicle") extracellular fluid; finally, the originally single vesicle-related crystals fuse into larger crystal clusters of up to hundreds of nanometers size (Cuisinier, 1996). In addition, the osteoblastic cells excrete organic matrix called osteoid (Parfitt, 1983; Skinner and Jahren, 2007), which is composed of 300 nm long and 1 nm thick strand-type collagen molecules. These molecules self-assemble into higher organizational units called fibrils, with typical diameters of tens to hundreds of nanometers, and lengths reaching even millimeters, leaving some extrafibrillar space in between. Within the fibrils, 280 nm long overlap regions (with dense collagen packing), alternate with 40 nm long gap regions (with loose collagen packing), forming a staggered scheme discovered by Hodge and Petruska (1963). Collagen deposition and hydroxyapatite mineralization are separated in time and space (Parfitt, 1983), such that the organic matrix, some ten to twenty days after the deposition, starts to become mineralized. Transmission electron micrographs showed that mineral precipitation occurs both intrafibrillarly and extrafibrillarly, but that, as a rule, the majority of the mineral is found in the extrafibrillar space (Hellmich and Ulm, 2003; Lees and Prostak, 1988; Lees et al., 1994; Prostak and Lees, 1996; McNally et al., 2012; Alexander et al., 2012; Jantou et al., 2009; Jantou-Morris et al., 2010).

This short summary clearly shows that, up to now, bone mineralization has been mainly studied experimentally, aiming at the deciphering of fundamental mechanisms. Wishing to foster the current trend in biomaterial science to develop theoretical and

* Corresponding author. Tel.: +43 1 58801 20220; fax: +43 1 58801 20299.
E-mail addresses: Claire.morin@tuwien.ac.at (C. Morin), Christian.hellmich@tuwien.ac.at (C. Hellmich).

0022-5193
http://dx.doi.org/10.1016/j.jtbi.2013.06.018

Nomenclature

Variables

d	Neutron diffraction spacing
$\mathcal{D}$	Dessication degree
f	Volume fraction
m	Mass
$\mathcal{M}$	Mineralization degree
n	Amount
$\mathcal{R}$	Fluid-to-organic mass ratio
t	Time
V	Volume
ρ	Mass density

Prefix

Δ	Change of variable due to dehydration

Suffices

col	… of collagen
dry	… of dried tissue
ec	… of extracollagenous space
ef	… of extrafibrillar space
ef,fl	… of extrafibrillar fluid
ef,HA	… of extrafibrillar mineral
fib	… of fibrillar space
fib,fl	… of fibrillar fluid
fib,HA	… of fibrillar mineral
fl	… of fluid
HA	… of hydroxyapatite
max	Maximum of …
$tissue$	… of tissue (at the extracellular scale)
w	… of wet tissue

Superscripts

0	at the beginning of the mineralization process
∞	at the end of the mineralization process
dh	partially dehydrated
t	at time instant t, between the beginning and the end of the mineralization process
$\hat{\cdot}$	inside the fibrils
$\check{\cdot}$	in the extrafibrillar space
$\dot{a}$	temporal derivative of a

computational approaches to further pervade the matter, the present paper is concerned with finding mathematically formulated rules behind the aforementioned mineralization process within and outside the collagen fibrils. These rules will be strictly validated against a variety of physically and statistically independent experimental data collected from the rich literature on the topic. While the systems biology of bone, or the hierarchical microstructure of mineralized bone and its emerging mechanical properties have been studied quite successfully by theoretical and computational approaches (Lemaire et al., 2004; Qin and Swain, 2004; Fritsch and Hellmich, 2007; Hellmich et al., 2004; Pivonka et al., 2008), the *evolution* of the fibrillar collagen–mineral nanocomposite in the course of biomineralization has, to the best knowledge of the authors, at mostly faintly been addressed by means of mathematical modeling. As kind of première-type activity, we will test, throughout the remainder of this paper, the following proposition: bone mineralization is a closed thermodynamic process, both at the tissue level and at the fibrillar level, which is expressed by mass density increase and volume reduction.

2. Methods

2.1. Mass conservation during mineralization

We wish to check, whether the structural evolution of bone tissue during mineralization can be explained by means of fluid–solid phase transitions in two thermodynamically closed systems. Therefore, we consider a piece of extracellular bone tissue (at a scale of some tens of micrometers) with properties averaged over a classical bone sample measuring one to a few millimeters, as accessible through standard experimental protocols (Biltz and Pellegrino, 1969; Gong et al., 1964; Lees et al., 1979; Vuong and Hellmich, 2011). As reviewed in the introduction, such tissue is laid down (at time "0") in the form of osteoid, consisting of collagen molecules with mass m^0_{col}, and of a ionic fluid with mass m^0_{fl}. Hence, the overall tissue mass reads as:

$$m^0_{tissue} = m^0_{col} + m^0_{fl} \tag{1}$$

At a higher organizational level (see Fig. 1), the collagen molecules build up fibrils with mass m^0_{fib}, consisting of molecular collagen and intercollagenous fluid (with mass $m^0_{fib,fl}$), so that

$$m^0_{fib} = m^0_{col} + m^0_{fib,fl} \tag{2}$$

The rest of the osteoid tissue consists of fluid-filled extrafibrillar space with mass $m^0_{ef} = m^0_{ef,fl}$. Hence, the initial tissue mass can be alternatively written as

$$\begin{aligned} m^0_{tissue} &= m^0_{fib} + m^0_{ef} \\ &= m^0_{col} + m^0_{fib,fl} + m^0_{ef,fl} \end{aligned} \tag{3}$$

Thereafter, the ions swimming in the fluid start to form hydroxyapatite minerals (referred to by suffix "HA" in the sequel).

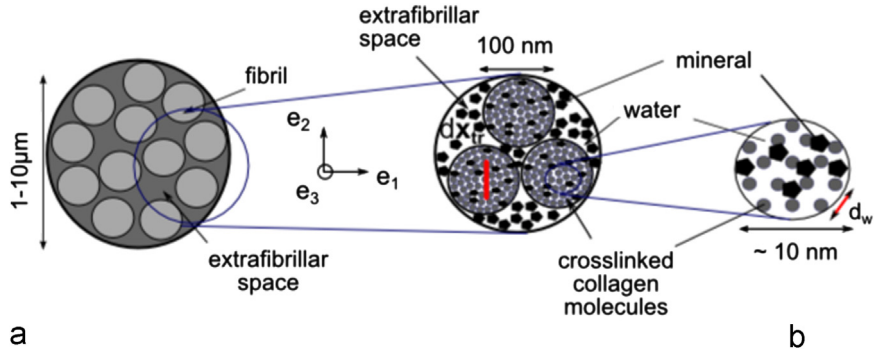

Fig. 1. Scheme concerning hierarchical structure of mineralizing bone tissue: (a) bone tissue and (b) fibrillar space.

If both the fibrils and the extrafibrillar space are closed thermodynamic systems (Coussy, 1995), i.e. if no fluid mass leaves or enters these volumes during the mineralization process, then the aforementioned precipitation of hydroxyapatite crystals entails that the mass rate of lost ionic fluid mass equals the mass rate of formed solid hydroxyapatite crystal mass in the fibrillar and extrafibrillar subvolumes, as well as in the entire tissue volume

$$\dot{m}_{fib,HA} = -\dot{m}_{fib,fl}$$
$$\dot{m}_{ef,HA} = -\dot{m}_{ef,fl}$$
$$\dot{m}_{HA} = -\dot{m}_{fl} \quad (4)$$

where a dot denotes the time derivative, and suffices "fib,HA" and "ef,HA" refer to the hydroxyapatite crystals formed in the fibrils and in the extrafibrillar space, respectively. At any time t of the mineralization process, integration of the relations (4) yields

$$m^t_{fib,fl} = m^0_{fib,fl} - m^t_{fib,HA}$$
$$m^t_{ef,fl} = m^0_{ef,fl} - m^t_{ef,HA}$$
$$m^t_{fl} = m^0_{fl} - m^t_{HA} \quad (5)$$

In particular, at the end of the mineralization process (at time "∞"), all the calcium and phosphate ions in the original ionic solution have formed solid hydroxyapatite, so that the remaining mass of the fluid in each compartment reads as

$$m^\infty_{fib,fl} = m^0_{fib,fl} - m^\infty_{fib,HA}$$
$$m^\infty_{ef,fl} = m^0_{ef,fl} - m^\infty_{ef,HA}$$
$$m^\infty_{fl} = m^0_{fl} - m^\infty_{HA} \quad (6)$$

On the other hand, the collagen mass remains unaltered throughout the mineralization process

$$m^0_{col} = m^\infty_{col} = m^t_{col} = m_{col} \quad (7)$$

so that Eqs. (1), (6), and (7) give access to the mass of each compartment at the end of the mineralization process

$$m^0_{fib} = m_{col} + m^0_{fib,fl} = m_{col} + m^\infty_{fib,fl} + m^\infty_{fib,HA} = m^\infty_{fib} = m_{fib}$$
$$m^0_{ef} = m^0_{ef,fl} = m^\infty_{ef,fl} + m^\infty_{ef,HA} = m^\infty_{ef} = m_{ef}$$
$$\Rightarrow m^0_{tissue} = m^\infty_{tissue} = m_{tissue} \quad (8)$$

Eq. (8) expresses that the overall mass of the tissue, but also the submasses of fibrils and extrafibrillar space remain constant throughout the entire mineralization process. In the following sections, we will check the relevance of propositions (1)–(8), by confronting them to numerous experimental data. This, however, requires a number of mathematical developments since, rather than masses [as occurring in Eqs. (1)–(8)], mass *densities* of tissues (see Table 1) are directly accessible from experiments. In addition, the precipitation of solved ions into solid mineral crystals is accompanied by an increase in mass density, which, upon overall mass preservation, leads to a *volume decrease* (or "shrinkage") of the tissues during the biomineralization process. This shrinkage affects both the fibrillar and the extrafibrillar tissue compartments, and the shrinkage of the fibrils can be experimentally accessed through equatorial neutron diffraction spacings d^∞_w measured on fully mineralized tissues (Morin et al., 2013; Miles and Ghelashvili, 1999)

$$\left(\frac{d^\infty_w}{d^0_w}\right)^2 = \frac{V^\infty_{fib}}{V^0_{fib}} \quad (9)$$

with d^0_w as the neutron diffraction spacing at the time of osteoid deposition ($t=0$), and V^0_{fib} and V^∞_{fib} as the fibrillar volume in unmineralized and fully mineralized tissues, respectively; see Table 1 for experimental values concerning d^∞_w.

Consequently, the remainder of this paper will be devoted to deriving, from Eqs. (1)–(9), a mass density–diffraction relation (ρ^∞_{tissue}–d^∞_w relation), in three consecutive steps: first, the mineralization-induced shrinkage will be evaluated at the tissue level, based on "universal" tissue composition rules evidenced in (Vuong and Hellmich, 2011); secondly, the mineralization-induced extrafibrillar volume change will be evaluated based on the on-average uniform mineral concentration in the extracollagenous space as evidenced in (Hellmich and Ulm, 2003) and on a hydration-dependent swelling rule for unmineralized tissues as evidenced in (Morin et al., 2013); and thirdly, an analogous procedure will allow for determination of the mineralization-driven shrinkage of the fibrils. The resulting ρ^∞_{tissue}–d^∞_w relation will be fed with experimental data for ρ^∞_{tissue} (from the second column of Table 1), and the corresponding predictions for diffraction spacings d^∞_w will be compared to the experimental data from the third column of Table 1. After this first "tissue-as-thermodynamically-closed-system" check, the developments will be extended to partially dehydrated tissues, based on data from Table 2; before general structural evolution patterns of mineralizing bone tissues will be shown and discussed.

Table 1
Experimental data: neutron diffraction spacings in wet and dry tissues, and corresponding extracellular mass densities.

Bone	Mass density of wet tissue ρ^∞_{tissue} [g/cm^3]	Diffraction spacing of wet tissue d^∞_w [nm]	Diffraction spacing of dried tissue d^∞_{dry} [nm]
Codfish clythrum[a]	1.44	1.38	1.07
Mineralized turkey tendon[a]	1.66	1.34	1.03
Mineralized turkey tendon[a]	1.58	1.33	1.08
Deer Antler[a]	1.80	1.29	1.11
Cow tibia[a]	2.04	1.24	1.16
Horse petrosal[b]	2.30	1.20	–
Whale t. bulla[b]	2.50	1.18	–
Porpoise petrosal[b]	2.70	1.115	–

[a] Lees et al. (1984).
[b] Lees (2003).

Table 2
Experimental data: neutron diffraction spacings in dehydrated tissues, and corresponding water contents, from (Lees and Mook, 1986). These experiments are performed on extracellular bone tissue with a mass density of $\rho^\infty_{tissue} = 2.1$ g/cm^3.

Water-to-organic mass ratio $\mathscr{R}^{\infty,dh}$ [-]	Diffraction spacing $d^{\infty,dh}_w$ [nm]
0	1.18
0.025	1.15
0.19	1.17
0.24	1.20
0.27	1.20
0.32	1.21
0.37	1.23
0.39	1.22
0.42	1.22
0.50	1.24
0.51	1.24
0.53	1.25
0.54	1.23
0.58	1.27

2.2. Mineralization-induced volume change at tissue level

The conservation of mass during the phase transformation from ionic fluid to solid hydroxyapatite, taking place under closed thermodynamic conditions according to Eq.$(6)_3$, together with the precipitation-induced mass density gain from the fluid state (with $\rho_{fl}=1.00\ \mathrm{g/cm^3}$) to the solid state [with the real mass density of (biologically generated, "impure") hydroxyapatite amounting to $\rho_{HA}=3.00\ \mathrm{g/cm^3}$ (Lees, 1987)], implies a decrease of the tissue volume during the mineralization process. This volume change at the tissue level can be quantified through

$$\frac{V^{\infty}_{tissue}}{V^{0}_{tissue}}=\frac{1}{1+(\rho_{HA}/\rho_{fl}-1)\times f^{\infty}_{HA}(\rho^{\infty}_{tissue})} \tag{10}$$

with f^{∞}_{HA} as the mineral volume fraction in the fully mineralized tissue, which depends on the tissue mass density, as given in Appendix A, Eq. (A.4). In more detail, Eq. (10) follows from expressing both initial and final volumes as functions of the constituent masses [see Eqs. (1) and (8)] and mass densities, and from subsequent expression of the constituent masses in terms of constituent volume fractions; the latter ones fulfilling "universal" compositional rules evidenced by Vuong and Hellmich (2011), see Appendix A for details.

2.3. Mineralization-induced volume change at extrafibrillar level

The most pronounced shrinkage effect of the compaction of mineral ions during precipitation of hydroxyapatite takes place at the level of the extrafibrillar space, which is, prior to mineralization, entirely filled by the ionic solution. The corresponding volume change can be quantified through

$$\frac{V^{\infty}_{ef}}{V^{0}_{ef}}=1+\frac{(1-\rho_{HA}/\rho_{fl})}{1-f^{0}_{col}}\frac{V^{\infty}_{tissue}}{V^{0}_{tissue}}\times f^{\infty}_{HA}(\rho^{\infty}_{tissue}) \tag{11}$$

where $V^{\infty}_{tissue}/V^{0}_{tissue}$ obeys Eq. (10), $f^{\infty}_{HA}(\rho^{\infty}_{tissue})$ still follows from Eq. (A.4), and f^{0}_{col} is the collagen volume fraction in unmineralized (osteoid) tissue, which can be quantified from the hydration-dependent swelling rules evidenced by Morin et al. (2013), see Appendix B, Eq. (B.5). As regards the structure of Eq. (11), its derivation rests upon conservation expression $(5)_2$ and upon the finding of Hellmich and Ulm (2003) that the mineral concentration in the extrafibrillar space is identical to that in the overall extracollageneous space (inside *and* outside the fibrils), see Appendix C for details.

2.4. Mineralization-induced volume change at fibrillar level

The mineralization-induced shrinkage of the bone tissue according to Eq. (10) can also be downscaled to the fibrillar level, by means of the fibrillar volume fraction $f_{fib}=V_{fib}/V_{tissue}$

$$\frac{V^{\infty}_{fib}}{V^{0}_{fib}}=\frac{f^{\infty}_{fib}}{f^{0}_{fib}}\frac{V^{\infty}_{tissue}}{V^{0}_{tissue}} \tag{12}$$

where

$$f^{\infty}_{fib}=1-f^{\infty}_{ef} \tag{13}$$

with f^{∞}_{ef} as the extrafibrillar volume fraction in the mineralized tissue, following from evaluation of (C.13) for $t\to\infty$, and f^{0}_{col} according to (B.5), so that, conclusively, the mass conservation law for a thermodynamically closed bone tissue as introduced in this paper, the on-average uniform hydroxyapatite concentration in the extracollagenous tissue spaces (Hellmich and Ulm, 2003), the bilinear composition rules for fully mineralized tissues (Vuong and Hellmich, 2011), and the hydration-dependent swelling rule for unmineralized collagenous tissues (Morin et al., 2013) allow for prediction of the fibrillar volume change just from known tissue mass densities, as collected in Table 1. In order to check the reliability of these predictions, they are transformed into neutron diffraction spacings, according to continuum geometry and considering negligible length changes in the meridional direction of the tissue (Morin et al., 2013), already expressed in Eq. (9), so that, thanks to Eqs. (12), (13), (A.4), (10), (C.13), (B.5)

$$d^{\infty}_{w}=d^{0}_{w}\sqrt{\frac{1-f^{0}_{ef}\times\left[1-(\rho_{HA}/\rho_{fl}-1)\times f^{\infty}_{HA}\times\dfrac{f^{\infty}_{col}}{\rho_{HA}f^{\infty}_{HA}/\rho_{fl}+f^{\infty}_{fl}}\right]}{(1-f^{0}_{ef})\times\left[1+(\rho_{HA}/\rho_{fl}-1)\times f^{\infty}_{HA}\right]}} \tag{14}$$

with f^{0}_{ef} according to Eq. (B.5), with $d^{0}_{w}=d_{max}=1.52$ nm [see Eq. (B.1)], and with dependencies of f^{∞}_{col}, f^{∞}_{HA}, and f^{∞}_{fl} on tissue mass density as in (A.4). Eq. (14), together with Eqs. (B.5) and (A.4), finally allows for a full quantitative check of our proposition of considering mineralizing bone tissue compartments as closed thermodynamic systems: its right-hand side is fed with the tissue mass density values of the second column of Table 1, and the resulting diffraction values are compared to the experimental values of the third column of Table 1.

2.5. Drying-induced volume change of mineralized tissues

As a complementary check of our mineralization rule, we consider partially dehydrated and fully dried tissues (indicated by superscript "dh" standing for dehydrated), whose water-to-organic mass ratios $\mathscr{R}^{\infty,dh}$ and neutron diffraction spacings $d^{\infty,dh}_{w}$ were recorded and documented (Lees and Mook, 1986), see Table 2 and the last column of Table 1. During dehydration, some fluid mass Δm^{∞}_{fl} and corresponding volume ΔV^{∞}_{fl} are lost, so that, with respect to the fully mineralized state, the tissue shrinks again, whereby the respective volume change reads as

$$\frac{V^{\infty}_{tissue}-\Delta V^{\infty}_{fl}}{V^{\infty}_{tissue}}=\frac{V^{\infty,dh}_{tissue}}{V^{\infty}_{tissue}}=1-\Delta f^{\infty}_{fl} \tag{15}$$

In Eq. (15), Δf^{∞}_{fl} is that volume fraction of fluid in a fully mineralized bone tissue, which will be lost due to dehydration: $\Delta f^{\infty}_{fl}\leq f^{\infty}_{fl}$, where the equal sign refers to the fully dehydrated case. Accordingly, the constituent volume fractions of the partially or fully dehydrated tissue read as

$$f^{\infty,dh}_{fl}=\frac{f^{\infty}_{fl}-\Delta f^{\infty}_{fl}}{1-\Delta f^{\infty}_{fl}}$$

$$f^{\infty,dh}_{col}=\frac{f^{\infty}_{col}}{1-\Delta f^{\infty}_{fl}}$$

$$f^{\infty,dh}_{HA}=\frac{f^{\infty}_{HA}}{1-\Delta f^{\infty}_{fl}} \tag{16}$$

In order to downscale (15) to the fibrillar level (where we seek experimental validation through diffraction data), we need to know how the lost fluid volume ΔV^{∞}_{fl} is partitioned between the fibrillar and extrafibrillar spaces. Therefore, we again consider the identity of extrafibrillar and extracollageneous mineral concentrations (Hellmich and Ulm 2003), as given in detail in Appendix D. This finally allows for identification of the dehydration-induced fibrillar shrinkage, according to

$$\frac{V^{\infty,dh}_{fib}}{V^{\infty}_{fib}}=\frac{V^{\infty}_{fib}-\Delta V^{\infty}_{fib,fl}}{V^{\infty}_{fib}}=\frac{V^{\infty}_{fib}-(\Delta V^{\infty}_{ec}-\Delta V^{\infty}_{ef})}{V^{\infty}_{fib}}\times\frac{V^{\infty}_{tissue}}{V^{\infty}_{tissue}}$$
$$=1-\frac{\Delta f^{\infty}_{fl}}{f^{\infty}_{fib}}\times\left(1-\frac{f^{0}_{ef}}{1-f^{0}_{col}}\right) \tag{17}$$

This model prediction for the dehydration-induced shrinkage can be experimentally validated, again by means of diffraction data,

analogously to Eq. (9)

$$\frac{V_{fib}^{\infty,dh}}{V_{fib}^{\infty}} = \left(\frac{d_w^{\infty,dh}}{d_w^{\infty}}\right)^2 \tag{18}$$

Combination of (18) and (17), reading as

$$d_w^{\infty,dh} = d_w^{\infty}\sqrt{1-\frac{\Delta f_{fl}^{\infty} - f_{ef}^0 \Delta f_{fl}^{\infty}/(1-f_{col}^0)}{f_{fib}^{\infty}}} \tag{19}$$

provides a second fully independent quantitative check of our proposition of considering bone tissue compartments as closed thermodynamic systems, also under dehydration. Accounting for

$$\Delta f_{fl}^{\infty} = f_{fl}^{\infty} - \mathscr{R}^{\infty,dh} f_{col}^{\infty}\frac{\rho_{col}}{\rho_{fl}} \tag{20}$$

the right-hand side of (19) is fed with fluid-to-organic mass ratios $\mathscr{R}^{\infty,dh}$, according to the first column of Table 2, and the resulting diffraction values are compared to the experimental values of the second column of Table 2. Identification of $\Delta f_{fl}^{\infty} = f_{fl}^{\infty}$ in (19) delivers model predictions for the diffraction spacing in fully dried tissue as

$$\begin{aligned} d_{dry}^{\infty} &= d_w^{\infty}\sqrt{1-f_{fl}^{\infty}} \\ &= d_w^0\sqrt{1-f_{fl}^{\infty}}\sqrt{\frac{1-f_{ef}^0\times\left[1-(\rho_{HA}/\rho_{fl}-1)f_{HA}^{\infty}\times\frac{f_{col}^{\infty}}{f_{HA}^{\infty}\rho_{HA}/\rho_{fl}+f_{fl}^{\infty}}\right]}{(1-f_{ef}^0)\times\left[1+(\rho_{HA}/\rho_{fl}-1)\times f_{HA}^{\infty}\right]}} \end{aligned} \tag{21}$$

with f_{ef}^0 according to Eq. (B.5) and mass density-dependent volume fractions $f_{col}^{\infty}, f_{HA}^{\infty}$, and f_{fl}^{∞} according to (A.4). Eq. (21) will be checked through the data pairs of columns 2 and 4 of Table 1. All aforementioned comparisons, checking the proposed mass conservation rules, are quantified in terms of relative errors between theoretical predictions d^{pred} of the diffraction spacings [Eqs. (14), (19), and (21), together with (20), (A.4), and (B.5)] and corresponding experimental values d^{exp} from Tables 1 and 2

$$e_d = \frac{d^{pred}-d^{exp}}{d^{exp}} \tag{22}$$

2.6. Evolution of tissue composition and structure during mineralization

We here derive mathematical expressions for the tissue compartment volume changes as well as for the constituent volume fractions, as functions of the mineralization degree, defined as:

$$\mathscr{M} = \frac{n_{HA}^t}{n_{HA}^{\infty}} = \frac{V_{HA}^t}{V_{HA}^{\infty}} = \frac{m_{HA}^t}{m_{HA}^{\infty}} \tag{23}$$

with n_{HA}^t and n_{HA}^{∞} as the amount of hydroxyapatite (typically measured in moles) in the tissue at time t and at time "∞", respectively. Use of mass–volume relation (A.3) specified for time t instead of "∞", in mass balance Eq. $(5)_3$, followed by the insertion of the result into the volume composition at time t, which follows from replacing "∞" by "t" in Eq. (A.2), and identification of the initial volume composition given by Eq. (A.1), yields

$$\frac{V_{tissue}^t}{V_{tissue}^0} = 1-\mathscr{M} f_{HA}^{\infty}\frac{V_{tissue}^{\infty}}{V_{tissue}^0}\times\left(\frac{\rho_{HA}}{\rho_{fl}}-1\right) \tag{24}$$

where $V_{tissue}^{\infty}/V_{tissue}^0$ still follows from Eq. (10).

Similarly, the extrafibrillar volume change due to mineralization follows from the insertion of Eq. (C.13) into Eq. (C.1) specified for time t instead of "∞"

$$\frac{V_{ef}^t}{V_{ef}^0} = 1+\frac{(1-\rho_{HA}/\rho_{fl})}{1-f_{col}^0}\frac{V_{HA}^t}{V_{tissue}^0} = 1+\frac{(1-\rho_{HA}/\rho_{fl})}{1-f_{col}^0}\mathscr{M} f_{HA}^{\infty}\frac{V_{tissue}^{\infty}}{V_{tissue}^0} \tag{25}$$

Analogously, the fibrillar volume change reads as

$$\frac{V_{fib}^t}{V_{fib}^0} = \frac{f_{fib}^t}{f_{fib}^0}\frac{V_{tissue}^t}{V_{tissue}^0} = \frac{1-f_{ef}^t}{f_{fib}^0}\frac{V_{tissue}^t}{V_{tissue}^0} \tag{26}$$

When accounting additionally for Eq. (B.3) and for Eq. (C.13) we arrive at

$$\frac{V_{fib}^t}{V_{fib}^0} = \frac{1}{f_{fib}^0}\left[\frac{V_{tissue}^t}{V_{tissue}^0} - f_{ef}^0 - \frac{f_{ef}^0\times(1-\rho_{HA}/\rho_{fl})}{1-f_{col}^0}\frac{V_{tissue}^{\infty}}{V_{tissue}^0}\mathscr{M} f_{HA}^{\infty}\right] \tag{27}$$

where $V_{tissue}^t/V_{tissue}^0$ is given in Eq. (24), f_{col}^0 and f_{ef}^0 are given in Eq. (B.5), and $f_{fib}^0 = 1-f_{ef}^0$ [see Eq. (B.3)].

As to derive a mineralization degree-dependent expression for the extrafibrillar volume fraction f_{ef}^t, we remember $f_{HA}^{\infty} = V_{HA}^{\infty}/V_{tissue}^{\infty}$ and (23), from which we get the relation

$$f_{HA}^t = \mathscr{M} f_{HA}^{\infty}\frac{V_{tissue}^{\infty}}{V_{tissue}^t} \tag{28}$$

We then insert Eq. (28) into Eq. (C.13), yielding

$$f_{ef}^t = \frac{f_{ef}^0}{V_{tissue}^t/V_{tissue}^0} + \frac{f_{ef}^0}{1-f_{col}^0}\times\left(1-\frac{\rho_{HA}}{\rho_{fl}}\right)\mathscr{M} f_{HA}^{\infty}\frac{V_{tissue}^{\infty}}{V_{tissue}^t} \tag{29}$$

In (29), f_{col}^0 and f_{ef}^0 follow from Eq. (B.5), f_{HA}^{∞} from Eq. (A.4), and $V_{tissue}^t/V_{tissue}^0$ from Eq. (24).

In order to get access to the expression $V_{tissue}^{\infty}/V_{tissue}^t$ as function of $\mathscr{M}$, we specify (A.2) for "t" instead of "∞", then replace m_{fl}^t by the expression given in $(5)_3$, followed by substitution of m_{fl}^0 by the expression following from $(6)_3$, yielding

$$\begin{aligned} V_{tissue}^t &= \frac{m_{col}}{\rho_{col}} + \frac{m_{fl}^{\infty}+m_{HA}^{\infty}-m_{HA}^t}{\rho_{fl}} + \frac{m_{HA}^t}{\rho_{HA}} \\ &= V_{tissue}^{\infty} + (m_{HA}^{\infty}-m_{HA}^t)\left(\frac{1}{\rho_{fl}}-\frac{1}{\rho_{HA}}\right) \end{aligned} \tag{30}$$

where we made use of the expression for V_{tissue}^{∞} according to (A.2). Using additionally definition (23) for the mineralization degree $\mathscr{M}$ and mass–volume relation $(A.3)_2$, we arrive at the sought relation

$$\frac{V_{tissue}^{\infty}}{V_{tissue}^t} = \frac{1}{1+(\rho_{HA}/\rho_{fl}-1)\times f_{HA}^{\infty}(\rho_{tissue}^{\infty})\times(1-\mathscr{M})} \tag{31}$$

As in Eq. (B.2), the collagen volume fraction within a fibril is the ratio between the collagen volume fraction within the tissue and the fibrillar volume fraction within the tissue, reading at time t as

$$\hat{f}_{col}^t = \frac{f_{col}^{\infty}}{f_{fib}^t}\frac{V_{tissue}^{\infty}}{V_{tissue}^t} \tag{32}$$

with $f_{fib}^t = 1-f_{ef}^t$ as given in Eq. (29), $V_{tissue}^{\infty}/V_{tissue}^t$ in Eq. (31), and f_{col}^{∞} in Eq. (A.4). The mineral volume fraction inside the fibrils, $\hat{f}_{HA}^t$, is determined by dividing the overall tissue volume fraction of fibrillar mineral, which is determined as the difference between the total and the extrafibrillar mineral volume fractions [given in Eq. (C.12)], by the volume fraction of the fibrils, f_{fib}^t

$$\hat{f}_{HA}^t = \frac{f_{HA}^t - f_{ef,HA}^t}{f_{fib}^t} = \frac{1-f_{ef}^0/(1-f_{col}^0)}{f_{fib}^t}\mathscr{M} f_{HA}^{\infty}\frac{V_{tissue}^{\infty}}{V_{tissue}^t} \tag{33}$$

Finally, the volume fraction of fluid inside the fibrils reads as:

$$\hat{f}_{fl}^t = 1-\hat{f}_{HA}^t-\hat{f}_{col}^t \tag{34}$$

The volume fraction of mineral in the extrafibrillar space $\check{f}_{HA}^t$ is the ratio of the extrafibrillar mineral volume fraction [given in Eq. (C.12)] and the extrafibrillar volume fraction

$$\check{f}_{HA}^t = \frac{f_{ef,HA}^t}{f_{ef}^t} = \frac{f_{ef}^t}{f_{ef}^t\times(1-f_{col}^0)}\mathscr{M} f_{HA}^{\infty}\frac{V_{tissue}^{\infty}}{V_{tissue}^t} \tag{35}$$

and the volume fraction of fluid in the extrafibrillar space finally

reads as

$$\check{f}^t_{fl} = 1 - \check{f}^t_{HA} \tag{36}$$

3. Results

3.1. Mineralizing bone tissue as closed thermodynamic system: experimental validation

In order to check the relevance of representing mineralizing bone tissue as a thermodynamically closed system, in which hydroxyapatite precipitates from an ionic solution filling all extracollagenous spaces (both intra- and extrafibrillarly), we compare the mathematical model-predicted neutron diffraction spacings in mineralized tissues at different hydration states, according to Eqs. (14), (19), and (21) [together with Eqs. (A.4), (B.5), and (20)], to corresponding experimental values given in Tables 1 and 2, see Fig. 2. The remarkable precision of our mathematical approach is quantified through the relative error between model predictions and experimental values [see Eq. (22)], amounting to $e_d = 2.25\,\% \pm 2.51\,\%$ (mean value $\pm$ standard deviation).

3.2. Volume changes during mineralization and dessication

Given this excellent confirmation of hydroxyapatite precipitating under closed thermodynamic conditions from an ionic solution in the fibrillar and extrafibrillar spaces of bone tissue, the corresponding evolution Eqs. (24)–(27) [together with Eqs. (A.4), (10), (B.3), and (B.5)] can now be employed as to quantify the structural (volumetric) evolution of mineralizing bone tissue: during mineralization, the volume of the overall collagenous tissue is shrinking because the mass density of hydroxyapatite is around three times larger than that of the liquid ionic solution. In general, the more mineral is present in the tissue (i.e. the higher the mass density of the mineralized tissue or the higher the mineralization degree), the higher the shrinkage of the volumes of the different compartments (see Figs. 3 and 4). More specifically, this volume loss is minimal for low-mineralized tissues at the beginning of the mineralization process (see left lower corner of Fig. 3), whereas highly mineralized bone tissue has lost up to 60% of its initial (osteoid) volume (see right upper corner of Fig. 3). The overall tissue shrinkage due to mineralization is essentially a consequence of the shrinkage of the extrafibrillar space which looses, in highly mineralized tissues, more than 60% of its initial size [see Fig. 4(b)],

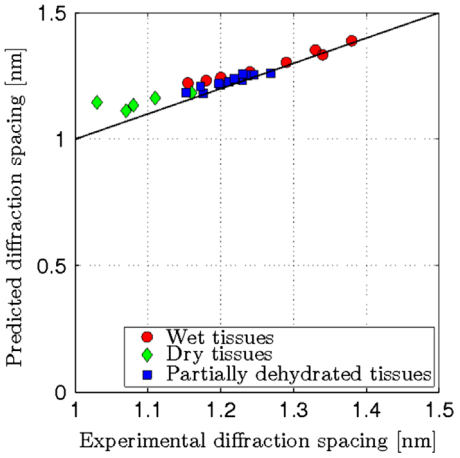

Fig. 2. Predicted vs. experimental diffraction spacing for wet, dry, and partially dehydrated, mineralized tissues. Experimental data are summarized in Tables 1 and 2.

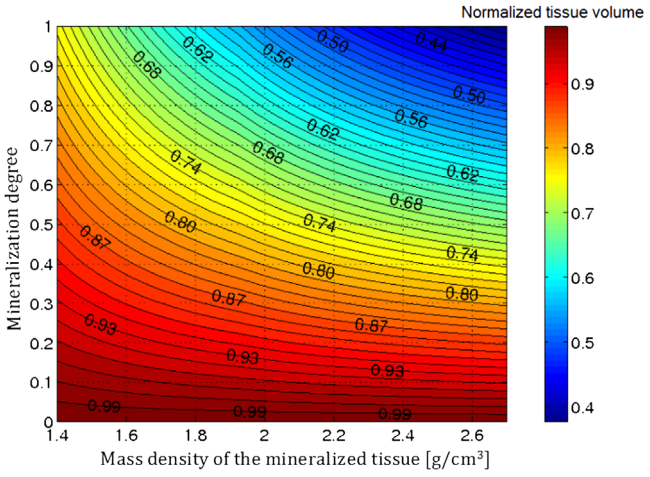

Fig. 3. Normalized tissue volume $V^t_{tissue}/V^0_{tissue}$ as function of the mineralization degree $\mathcal{M}$, for different final tissue mass densities ρ^{∞}_{tissue}.

all the more so as the extrafibrillar space makes up more than half of the volume of the initially non-mineralized tissue. During the mineralization period, the collagenous volume only reduces by slightly more than 30% [see Fig. 4(a)], due to the presence of (chemically inert) collagen in this compartment.

All these shrinkage and compaction phenomena are schematically illustrated in Fig. 5, where the volume changes are represented as changes in area, and where the local mass densities are quantified through a grey scale.

Fibrillar volume change is closely connected to the evolving equatorial diffraction spacing d^t_w [remember Eq. (9)], which can be predicted through Eq. (14) (in which superscript "∞" has to be replaced by t), together with Eqs. (28), (29), (31), (32), (A.4), and (B.5), for different tissues at different mineralization states (see Fig. 6). The diffraction spacing decreases with increasing mineralization degree (up to 20% for hyper dense bones of porpoise with $\rho^{\infty}_{tissue} = 2.7\ \mathrm{g/cm^3}$). It is also illustrative to plot dehydration-induced changes in the neutron diffraction spacings, according to Eq. (21), see Fig. 7. Our model predicts the diffraction spacing to decrease with the mass density of wet tissues, but to increase with the mass density of dry tissues, and this is what Lees (2003) observed experimentally.

3.3. Mineralization-induced compositional changes

Still motivated by the excellent model prediction capabilities shown in Fig. 2, we now use Eqs. (29) and (32)–(36), together with (31), (A.4), and (B.5), for illustrating the compositional evolutions of mineralizing bone tissues: The mineralization process leads to slight increase of the fibrillar volume fractions (up to about 20%, see Fig. 8), since the fibrils, thanks to the presence of chemically inert collagen, are less affected by the fluid-to-crystal transformation-induced volume loss, as compared to the extrafibrillar space.

Within the fibrils, the fluid volume fraction, starting from around 50% in the unmineralized osteoid, is reduced by one third in the case of low-mineralized tissues [see Fig. 9(a)], while it is almost completely consumed in the case of very highly mineralized tissues [see Fig. 9(d)]. Thereby, "lost" fluid volume fractions are "replaced" by collagen and mineral volume fractions, at about same shares [see Fig. 9(a)–(d)].

In the extrafibrillar space, mineral volume fractions increase overlinearly with the mineralization degree, the more so the more highly the tissue is mineralized [see Fig. 10(a)–(d)].

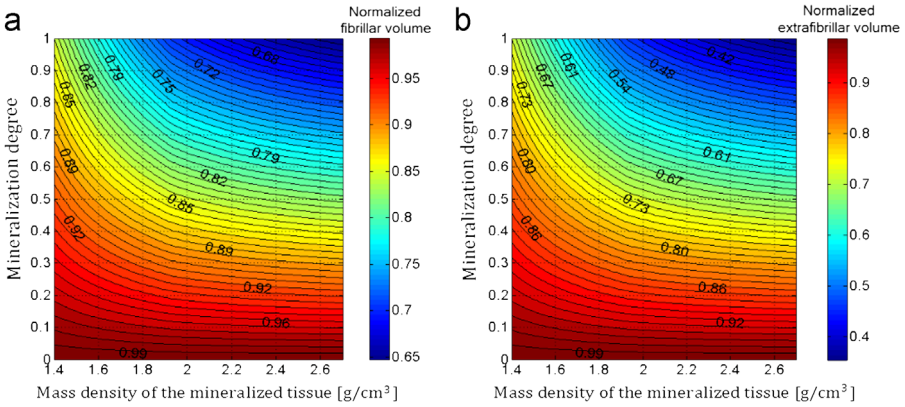

Fig. 4. Normalized fibrillar (a) and extrafibrillar (b) volumes, V^t_{fib}/V^0_{fib} (a) and V^t_{ef}/V^0_{ef} (b), as functions of the mineralization degree $\mathscr{M}$, for different final tissue mass densities ρ^{∞}_{tissue}.

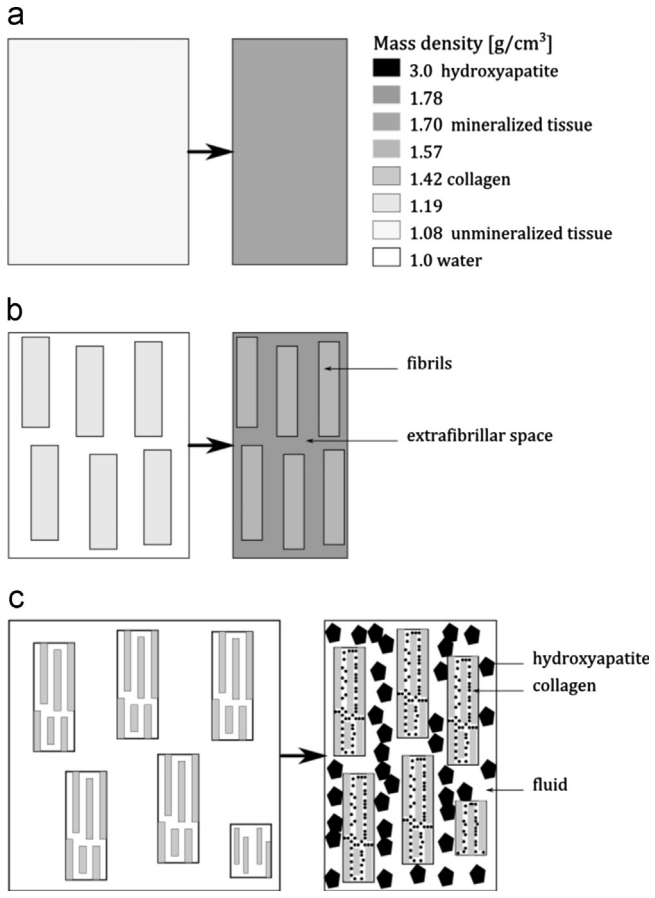

Fig. 5. Scheme of the structural evolution of extracellular bone tissue due to mineralization ($\rho^{\infty}_{tissue} = 1.70\,\mathrm{g/cm^3}$): the left structural schemes refer to the unmineralized state, and the right ones refer to fully mineralized tissue: (a) tissue scale, (b) compartment (fibrillar) scale, (c) collagen–mineral scale; grey scale indicates mass densities of tissues and tissue constituents.

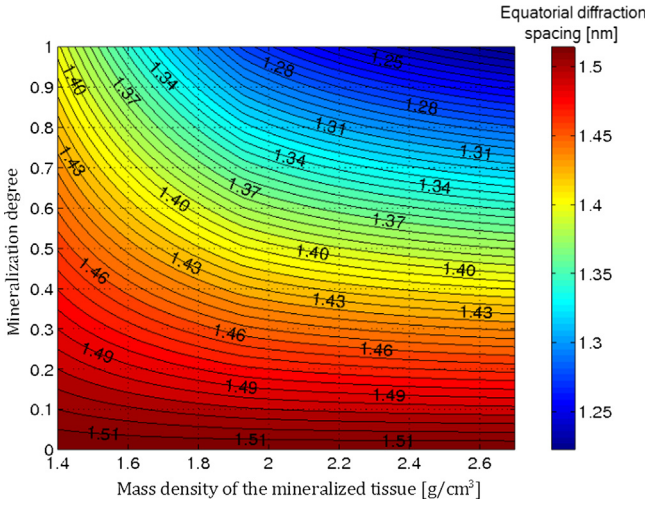

Fig. 6. Equatorial diffraction spacing d^t_w, as function of the mineralization degree $\mathscr{M}$, for different mass densities of the mineralized tissues ρ^{∞}_{tissue}.

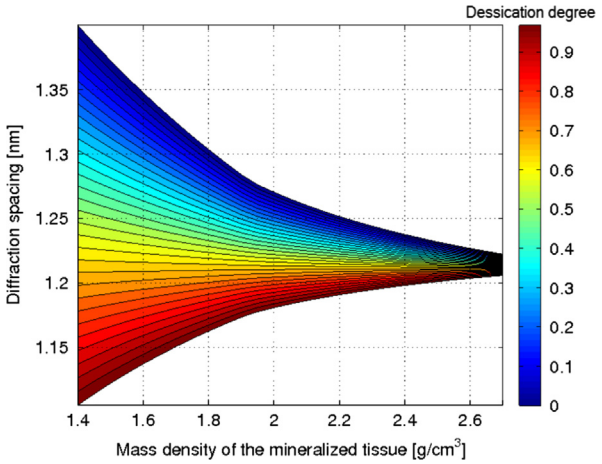

Fig. 7. Equatorial diffraction spacing $d^{\infty,dh}_w$, as function of the extracellular mass density of bone tissue ρ^{∞}_{tissue}, for different dessication degrees $\mathcal{D} = \Delta f^{\infty}_{fl}/f^{\infty}_{fl}$ ranging from 0% up to 100%.

4. Discussion

This contribution showed that the volume and structure changes in mineralizing bone tissue can be mathematically predicted when considering the tissue as a closed thermodynamic system, in which crystals start to precipitate from a supersaturated solution, while the mass conservation law is continuously fulfilled. The corresponding mathematical formulation incorporated earlier general findings on collagen swelling (Morin et al., 2013), on tissue composition at the fully mineralized state (Vuong and Hellmich, 2011), and on the partitioning of the mineral between the fibrillar

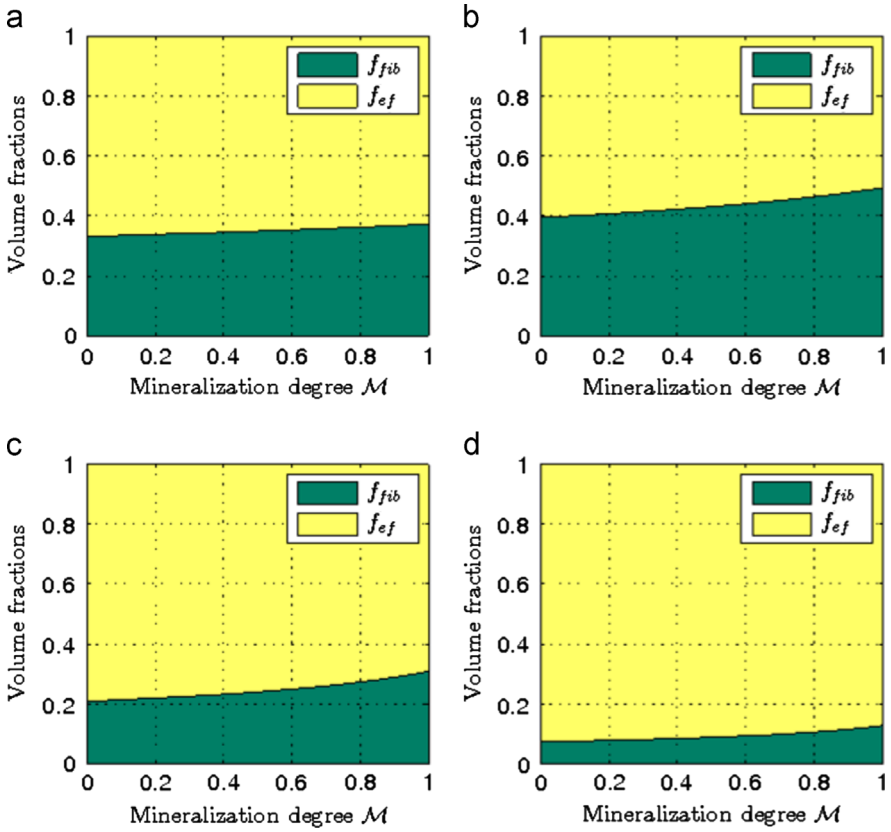

Fig. 8. Extrafibrillar and fibrillar volume fractions (f_{ef} and f_{fib}, respectively), as functions of the mineralization degree $\mathcal{M}$, for four different values of the extracellular tissue mass density ρ^{∞}_{tissue}: (a) ρ^{∞}_{tissue} =1.44 g/cm^3, (b) ρ^{∞}_{tissue} =1.90 g/cm^3, (c) ρ^{∞}_{tissue} =2.30 g/cm^3 and (d) ρ^{∞}_{tissue} =2.70 g/cm^3.

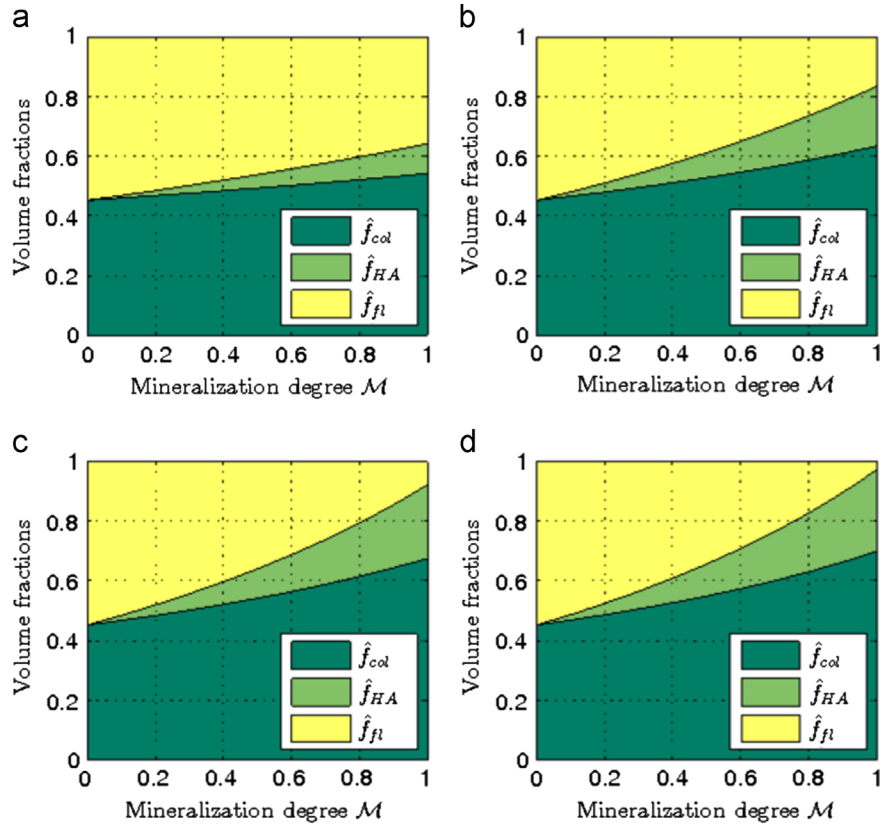

Fig. 9. Volume fractions of collagen, mineral, and water inside the fibrils ($\hat{f}_{col}$, $\hat{f}_{HA}$, and $\hat{f}_{fl}$, respectively), as functions of the mineralization degree $\mathcal{M}$, for four different values of the extracellular tissue mass density ρ^{∞}_{tissue}: (a) ρ^{∞}_{tissue} =1.44 g/cm^3, (b) ρ^{∞}_{tissue} =1.90 g/cm^3, (c) ρ^{∞}_{tissue} =2.30 g/cm^3 and (d) ρ^{∞}_{tissue} =2.70 g/cm^3.

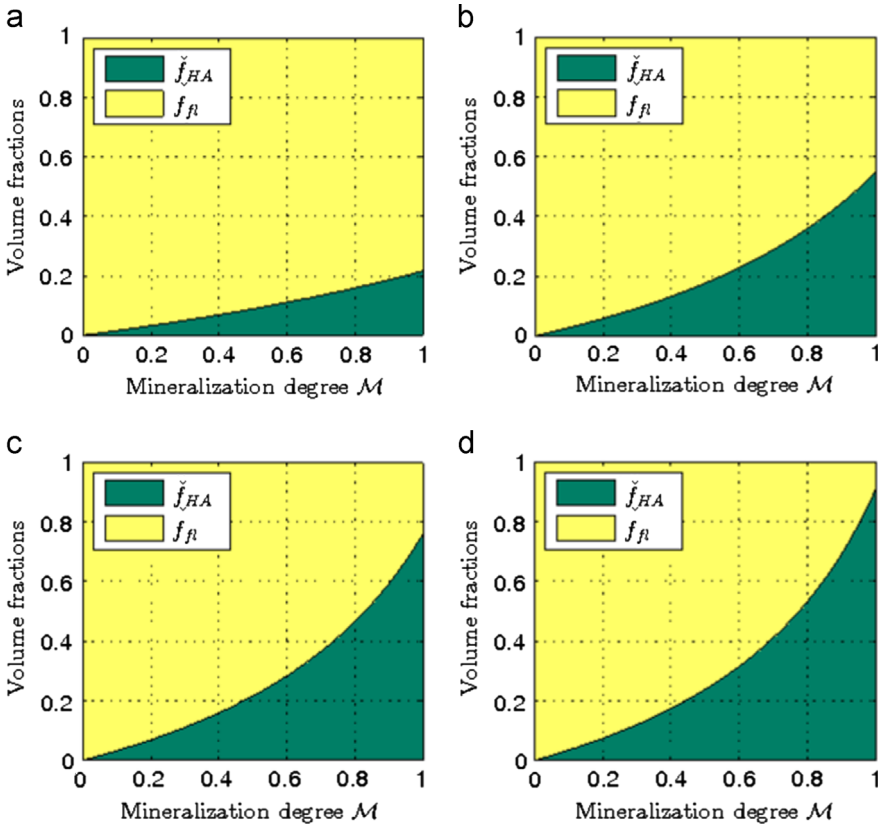

Fig. 10. Volume fractions of mineral and water inside the extrafibrillar space ($\check{f}_{HA}$, and $\check{f}_{fl}$, respectively), as functions of the mineralization degree $\mathcal{M}$, for four different values of the extracellular tissue mass density ρ^{∞}_{tissue}: (a) ρ^{∞}_{tissue} =1.44 g/cm^3, (b) ρ^{∞}_{tissue} =1.90 g/cm^3, (c) ρ^{∞}_{tissue} =2.30 g/cm^3 and (d) ρ^{∞}_{tissue} =2.70 g/cm^3.

and extrafibrillar spaces (Hellmich and Ulm, 2003). Our mathematical model was checked through various experimental data from neutron diffraction and mass density measurements at different mineralization and dehydration states. As regards the appropriate use of the used experimental data, we note that neutron diffraction is a well-accepted technique for micro-strain quantification (Daymond and Priesmeyer, 2002), and that millimeter-sized pieces of bone tissue exhibit a mean tissue age of the order of years (Baroncelli et al., 1998), which is much larger than the characteristic times of both primary and secondary mineralization, amounting to days (Wergedal and Baylink, 1974) and months (Bala et al., 2010). Therefore, such pieces give indeed access to the mass density ρ^{∞}_{tissue} of fully mineralized tissue.

In the bone tissues identified as closed thermodynamic systems, the volume of ionic solution involved in the precipitation process is fully replaced by the volume of newly formed mineral, and the potential relevance of such a replacement process of an originally larger volume of a low density substance, by a then smaller volume of a high density substance, was at least partially perceived by some researchers for quite some while: e.g., Deakins (1942) writes that "the volume of ash deposited just fills the space from which the water was displaced"; and Lees (2003) concludes that his diffraction-based calculation "where the mass of the tissue is constant and the volume varies, matches the results observed experimentally". As a major complement to these early "feelings", the present contribution, besides from being supported by an unprecedented number of independent experimental data, provides mathematical predictions of fibrillar and extrafibrillar, as well as mineral and collagen volumes and volume fractions, i.e. our general approach covers compositional changes at different hierarchical levels, throughout the bone mineralization process. Thereby, as a formal limitation of the present contribution, the complex chemical changes in the solid crystals, from hydroxyapatite precursors to hydroxyapatite itself (Cuisinier, 1996) are not explicitly modeled, i.e. "hydroxyapatite" in our model refers to "hydroxyapatite and all its precursors". In this context, we here leave aside a more detailed chemical description of hydroxyapatite precipitation, which is a very complex process depending with high sensitivity on chemical parameters (Orlovskii et al., 2002), the precise functioning of which *in vivo* is still in the discovery phase (Colfen, 2010). On the other hand, the time instants "0" and "infinity" as introduced in the present approach, can indeed be clearly assigned to the more detailed bone crystal growth mechanisms as introduced by Cuisinier (1996): "0" relates to crystal nucleation in the fluid spaces of a collagenous template which has already adsorbed the calcium and phosphate ions, while "infinity" relates to the completion of crystal fusion, following the intermediate crystal growth period.

Quantification of tissue volume and composition *evolution* during bone mineralization, as proposed in the present paper, provides valuable, new input values for computer-aided biomaterial design as an important complement to purely experimental approaches (Lindenmair et al., 2010; Verma et al., 2010). This newly emerging computational field has already provided tools for assessing the structural integrity of biomaterials and tissue-engineered bones, often based on Computed Tomography (CT) and Finite Element analyses (Lacroix et al., 2006; Scheiner et al., 2009), but also comprising analytical approaches (Bertrand and Hellmich 2009; Fritsch et al., 2010; Orr et al., 2003), as well as techniques for assessing or simulating the evolution of biomaterials and their surrounding tissues, with respect to bone ingrowth (Byrne et al., 2007; Sandino et al., 2008; Sandino and Lacroix, 2011; Sengers et al., 2007), scaffold degradation (Bohner and Baumgart, 2004), or chemically-induced biomaterial shrinkage (Orr et al., 2003). While, in all these approaches, bone tissue (be it natural or tissue-engineered), is considered as a non-evolving

entity, an assumption which may appear plausible for the applications discussed in the aforementioned references, our new results on mineralization-induced bone microstructure *evolution* now open the door towards the mechanical properties of *mineralizing* bone tissue (which can be derived from the volume fraction evolutions of Figs. 8–10), by means of experimentally validated micromechanics models (Hellmich et al., 2004; Fritsch and Hellmich, 2007; Fritsch et al., 2009; Hamed and Jasiuk, 2012), which, together with the tissues' shrinkage behavior illustrated in Figs. 3–5, will enable again more realistic simulations of the loading of tissue engineering scaffolds, namely through accounting also for a shrinkage-induced loading portion, which has never been considered so far. Moreover, our findings can also help to elucidate the stresses evolving in newly deposited osteoid in the course of bone remodeling, thereby complementing recent simulation results based on a coupled systems biology-micromechanics theory (Scheiner et al., 2013; Pivonka et al., 2008; Lemaire et al., 2004).

5. Conclusion

Mineralizing bone tissue acts as a closed thermodynamic system undergoing a fluid-to-solid phase transformation in the extra-collagenous space. The corresponding rigorous mathematical approach was successfully validated through neutron diffraction and physical chemistry tests, and gives unprecedented access to compositional and structural changes in mineralizing bone tissue, at all final collagen-to-mineral ratios found in Nature. Besides from its impact on fundamental bone science, this approach promises to open new avenues in computer-aided biomaterials design, by delivering so far inaccessible input data needed for realistic modeling of the scaffold-tissue interaction.

Acknowledgment

Financial support of the European Research Council (ERC) through the project ERC-2010-StG 257023-MICROBONE "Multiscale poro-micromechanics of bone materials, with links to biology and medicine" is gratefully acknowledged.

Appendix A. Derivation of the expression for tissue shrinkage, Eq. (10)

The initial tissue volume follows from the initial tissue mass (1) and the mass densities of the fluid (approximated by that of water, $\rho_{fl}=1.00$ g/cm^3) and of molecular collagen [$\rho_{col}=1.42$ g/cm^3 (Lees, 1981; Lees and Heeley, 1981; Morin et al., 2013)]

$$V^0_{tissue}=V_{col}+V^0_{fl}=\frac{m_{col}}{\rho_{col}}+\frac{m^0_{fl}}{\rho_{fl}} \tag{A.1}$$

with V_{col} and V^0_{fl} as the (initial) volumes of collagen and fluid.

Analogously, the final tissue volume follows from the final tissue mass (8) and the mass densities of collagen, fluid, and hydroxyapatite [the latter amounting to $\rho_{HA}=3.00$ g/cm^3 (Lees, 1987)]

$$V^\infty_{tissue}=V_{col}+V^\infty_{fl}+V^\infty_{HA}=\frac{m_{col}}{\rho_{col}}+\frac{m^\infty_{fl}}{\rho_{fl}}+\frac{m^\infty_{HA}}{\rho_{HA}} \tag{A.2}$$

with V_{col}, V^∞_{fl}, and V^∞_{HA} as the (final) volumes of collagen, fluid, and hydroxyapatite, respectively.

The final constituent masses can be expressed in terms of constituent volume fractions $f^\infty_{col}=V_{col}/V^\infty_{tissue}$, $f^\infty_{HA}=V^\infty_{HA}/V^\infty_{tissue}$, and $f^\infty_{fl}=V^\infty_{fl}/V^\infty_{tissue}$

$$m_{col}=\rho_{col}V_{col}=\rho_{col}f^\infty_{col}V^\infty_{tissue}$$
$$m^\infty_{HA}=\rho_{HA}V^\infty_{HA}=\rho_{HA}f^\infty_{HA}V^\infty_{tissue}$$
$$m^\infty_{fl}=\rho_{fl}V^\infty_{fl}=\rho_{fl}f^\infty_{fl}V^\infty_{tissue} \tag{A.3}$$

and it has been shown by Vuong and Hellmich (2011) from a large experimental data base obtained from different chemical protocols spanning over 80 years of research (Lees et al., 1979; Lees and Page, 1992; Lees et al., 1995; Lees, 2003; Gong et al., 1964; Hammet, 1925; Burns, 1929; Biltz and Pellegrino, 1969), that these volume fractions follow universal bilinear rules depending on the extracellular mass density ρ^∞_{tissue} of the bone tissue

$$\begin{aligned}
&\text{if } \rho^\infty_{tissue}\le 1.928\ \text{g/cm}^3, && \text{if } \rho^\infty_{tissue}\ge 1.928\ \text{g/cm}^3,\\
&f^\infty_{HA}=\tfrac{1}{\rho_{HA}}(1.331\,\rho^\infty_{tissue}-1.398), && f^\infty_{HA}=\tfrac{1}{\rho_{HA}}(1.709\,\rho^\infty_{tissue}-2.127),\\
&f^\infty_{col}=\tfrac{0.9}{\rho_{col}}(0.381\,\rho^\infty_{tissue}-0.230), && f^\infty_{col}=\tfrac{0.9}{\rho_{col}}(-0.471\,\rho^\infty_{tissue}+1.412),\\
&f^\infty_{fl}=1-f^\infty_{col}-f^\infty_{HA}. && f^\infty_{fl}=1-f^\infty_{col}-f^\infty_{HA}.
\end{aligned} \tag{A.4}$$

Use of (A.3) in $(6)_3$, and insertion of the result into (A.1) and (A.2), delivers the mineralization-induced tissue volume change as Eq. (10) of Section 2.2, with $f^\infty_{HA}(\rho^\infty_{tissue})$ according to Eq. (A.4).

Appendix B. Derivation of the expressions for the constituent volume fractions of unmineralized tissues

The extrafibrillar and collagen volume fractions in unmineralized tissues, f^0_{ef} and f^0_{col}, depend on the tissue hydration states, as was identified by Morin et al. (2013) from diffraction data, vacuum drying, and mass measurements (Katz and Li 1973; Lees and Heeley, 1981; Meek et al., 1991; Rougvie and Bear, 1953). Namely, upon fibrillar saturation, as always encountered in osteoid, the volume fraction of collagen within the fibrils is constant and amounts to

$$\hat{f}^0_{col}=\frac{V^0_{col}}{V^0_{fib}}=0.88\left(\frac{d_{dry}}{d_{max}}\right)^2=0.88\left(\frac{1.09}{1.52}\right)^2=0.45 \tag{B.1}$$

with $d_{dry}=1.09$ nm (Lees et al., 1984) and $d_{max}=1.52$ nm (Brodsky et al., 1982; Lees et al., 1984; Eanes et al., 1970; Katz and Li, 1973) as the (X-ray) diffraction spacings of fully dried and fully saturated unmineralized collagenous tissues. $\hat{f}^0_{col}$ relates to f^0_{col} through

$$f^0_{col}=\frac{V_{col}}{V^0_{fib}}\frac{V^0_{fib}}{V^0_{tissue}}=\hat{f}^0_{col}f^0_{fib} \tag{B.2}$$

and the fibrillar and extrafibrillar volume fractions, f^0_{fib} and f^0_{ef} respectively, read as

$$f^0_{fib}=\frac{V^0_{fib}}{V^0_{tissue}}=\frac{1}{0.88}\left(\frac{d_{max}}{d_{dry}}\right)^2\frac{\rho_{fl}}{\mathscr{R}^0\rho_{col}+\rho_{fl}}=2.21\frac{\rho_{fl}}{\mathscr{R}^0\rho_{col}+\rho_{fl}}$$
$$f^0_{ef}=1-f^0_{fib} \tag{B.3}$$

with $\mathscr{R}^0$ as the water-to-organic mass ratio in the unmineralized tissue, which can be retrieved from mass conservation rule $(6)_3$ and mass–volume relation (A.3) as

$$\mathscr{R}^0=\frac{m^0_{fl}}{m_{col}}=\frac{m^\infty_{HA}+m^\infty_{fl}}{m_{col}}=\frac{\rho_{HA}f^\infty_{HA}(\rho^\infty_{tissue})+\rho_{fl}f^\infty_{fl}(\rho^\infty_{tissue})}{\rho_{col}f^\infty_{col}(\rho^\infty_{tissue})} \tag{B.4}$$

while Eqs. (B.1), (B.2), and (B.3) allow for expressing the initial volume fraction of collagen f^0_{col} and the initial extrafibrillar volume fraction f^0_{ef} as

$$f^0_{col}=\frac{f^\infty_{col}(\rho^\infty_{tissue})}{\frac{\rho_{HA}}{\rho_{fl}}f^\infty_{HA}(\rho^\infty_{tissue})+f^\infty_{fl}(\rho^\infty_{tissue})+f^\infty_{col}(\rho^\infty_{tissue})}$$
$$f^0_{ef}=1-\frac{1}{0.88}\left(\frac{d_{max}}{d_{dry}}\right)^2\frac{f^\infty_{col}(\rho^\infty_{tissue})}{\frac{\rho_{HA}}{\rho_{fl}}f^\infty_{HA}(\rho^\infty_{tissue})+f^\infty_{fl}(\rho^\infty_{tissue})+f^\infty_{col}(\rho^\infty_{tissue})} \tag{B.5}$$

whereby dependencies on tissue mass density in (B.4) and (B.5) follow (A.4).

Appendix C. Derivation of the expression for the extrafibrillar shrinkage, Eq. (11)

Mineralization-induced shrinkage of the tissue according to Eq. (10) can be formally downscaled to the extrafibrillar level (the extrafibrillar space filling volume V_{ef}), by introduction of the extrafibrillar volume fraction $f_{ef}=V_{ef}/V_{tissue}$,

$$\frac{V_{ef}^{\infty}}{V_{ef}^{0}}=\frac{f_{ef}^{\infty}}{f_{ef}^{0}}\frac{V_{tissue}^{\infty}}{V_{tissue}^{0}} \tag{C.1}$$

At any time instant t, the extrafibrillar space consists of fluid and mineralized parts, with volume fractions $f_{ef,fl}^{t}$ and $f_{ef,HA}^{t}$

$$f_{ef}^{t}=f_{ef,fl}^{t}+f_{ef,HA}^{t} \tag{C.2}$$

whereby the mineralized part does not exist yet at the beginning of the mineralization process ($t=0$)

$$\begin{aligned} f_{ef}^{0}&=f_{ef,fl}^{0}\\ V_{ef}^{0}&=V_{ef,fl}^{0} \end{aligned} \tag{C.3}$$

In order to get access to the volume fraction $f_{ef,fl}$ of the extrafibrillar fluid, we divide mass conservation expression $(5)_2$ by the mass density of fluid, ρ_{fl}, and by the tissue volume V_{tissue}^{t}, yielding

$$\frac{m_{ef,fl}^{t}}{\rho_{fl}V_{tissue}^{t}}=\frac{V_{ef,fl}^{t}}{V_{tissue}^{t}}=f_{ef,fl}^{t}=\frac{V_{ef}^{0}}{V_{tissue}^{t}}-\frac{m_{ef,HA}^{t}}{\rho_{fl}V_{tissue}^{t}} \tag{C.4}$$

Next, we express the right-hand term of (C.4) as function of volume fractions and tissue shrinkage $V_{tissue}^{t}/V_{tissue}^{0}$, by using the real mass density of hydroxyapatite ρ_{HA}

$$f_{ef,fl}^{t}=\frac{V_{ef}^{0}}{V_{tissue}^{0}}\frac{V_{tissue}^{0}}{V_{tissue}^{t}}-\frac{V_{ef,HA}^{t}}{V_{tissue}^{t}}\frac{\rho_{HA}}{\rho_{fl}}=\frac{f_{ef}^{0}}{V_{tissue}^{t}/V_{tissue}^{0}}-f_{ef,HA}^{t}\frac{\rho_{HA}}{\rho_{fl}} \tag{C.5}$$

Insertion of (C.5) into (C.2) yields the extrafibrillar volume fraction f_{ef}^{t} as function of only two unknowns, $f_{ef,HA}^{t}$ and f_{ef}^{0}, in the form

$$f_{ef}^{t}=\frac{f_{ef}^{0}}{V_{tissue}^{t}/V_{tissue}^{0}}+f_{ef,HA}^{t}\times\left(1-\frac{\rho_{HA}}{\rho_{fl}}\right) \tag{C.6}$$

In order to get access into the first of these two unknowns, the volume fraction of hydroxyapatite in the extrafibrillar space, $f_{ef,HA}^{t}$, we recall the finding of Hellmich and Ulm (2003) that the mineral concentration in the extrafibrillar space is equal to that in the extracollagenous space, which reads mathematically as

$$\forall\, t\in[0,\infty],\quad \frac{m_{HA}^{t}}{V_{ec}^{t}}=\frac{m_{ef,HA}^{t}}{V_{ef}^{t}} \tag{C.7}$$

with $V_{ec}^{t}=V_{tissue}^{t}-V_{col}$ as the extracollagenous volume at time t. Relation (C.7) was confirmed by transmission electromicrographs (Prostak and Lees 1996; Zylberberg et al., 1998), neutron diffraction data (Lees et al., 1984; Bonar et al., 1985), and chemical tests (Lees 1987; Biltz and Pellegrino. 1969; Lees and Page, 1992), see (Hellmich and Ulm 2003) for details. In order to study the effect of mass conservation in closed fibrillar and extrafibrillar spaces, expressed through Eq. (4), on the on-average uniform concentration of mineral in the extracollagenous tissue space, we differentiate Eq. (C.7) with respect to time, yielding

$$\dot{m}_{HA}^{t}V_{ef}^{t}+m_{HA}^{t}\dot{V}_{ef}^{t}=\dot{m}_{ef,HA}^{t}V_{ec}^{t}+m_{ef,HA}^{t}\dot{V}_{ec}^{t} \tag{C.8}$$

Considering the volume rates as the sum of fluid and mineral subvolume rates, and expressing the latter as ratios of fluid and mineral mass rates over corresponding real mass densities yields:

$$\begin{aligned} V_{ef}^{t}&=V_{ef,HA}^{t}+V_{ef,fl}^{t}=\frac{m_{ef,HA}^{t}}{\rho_{HA}}+\frac{m_{ef,fl}^{t}}{\rho_{fl}}\Rightarrow\dot{V}_{ef}^{t}=\frac{\dot{m}_{ef,HA}^{t}}{\rho_{HA}}+\frac{\dot{m}_{ef,fl}^{t}}{\rho_{fl}}\\ V_{ec}^{t}&=V_{HA}^{t}+V_{fl}^{t}=\frac{m_{HA}^{t}}{\rho_{HA}}+\frac{m_{fl}^{t}}{\rho_{fl}}\Rightarrow\dot{V}_{ec}^{t}=\frac{\dot{m}_{HA}^{t}}{\rho_{HA}}+\frac{\dot{m}_{fl}^{t}}{\rho_{fl}} \end{aligned} \tag{C.9}$$

Insertion of (C.9) into (C.8), specifying the corresponding result for mass transformation (4), and using mass balance (5) yields

$$\dot{m}_{HA}^{t}\left(V_{ef}^{t}-\frac{m_{ef,HA}^{t}}{\rho_{HA}}+\frac{m_{ef,fl}^{0}}{\rho_{fl}}-\frac{m_{ef,fl}^{t}}{\rho_{fl}}\right)=\dot{m}_{ef,HA}^{t}\left(V_{ec}^{t}-\frac{m_{HA}^{t}}{\rho_{HA}}+\frac{m_{fl}^{0}}{\rho_{fl}}-\frac{m_{fl}^{t}}{\rho_{fl}}\right) \tag{C.10}$$

Integration of Eq. (C.10) between time zero (where no mineral is present) and time t, while using the relations for the initial fluid volumes in the extrafibrillar space, $V_{ef,fl}^{0}=m_{ef,fl}^{0}/\rho_{fl}$, and in the whole tissue, $V_{fl}^{0}=m_{fl}^{0}/\rho_{fl}$, yields

$$m_{ef,HA}^{t}=\frac{V_{ef,fl}^{0}}{V_{fl}^{0}}m_{HA}^{t} \tag{C.11}$$

Now, we are in the position to finally get access to the extrafibrillar mineral volume fraction, through dividing Eq. (C.11) by the mineral mass density ρ_{HA} and the current tissue volume V_{tissue}^{t}, while dividing the initial fluid volumes $V_{ef,fl}^{0}$ and V_{fl}^{0} by the initial tissue volume V_{tissue}^{0}, which yields

$$\begin{aligned} \frac{m_{ef,HA}^{t}}{\rho_{HA}V_{tissue}^{t}}=\frac{V_{ef,HA}^{t}}{V_{tissue}^{t}}=f_{ef,HA}^{t}&=\frac{V_{ef,fl}^{0}/V_{tissue}^{0}}{V_{fl}^{0}/V_{tissue}^{0}}\frac{m_{HA}^{t}}{\rho_{HA}V_{tissue}^{t}}\\ &=\frac{V_{ef}^{0}/V_{tissue}^{0}}{(V_{tissue}^{0}-V_{col})/V_{tissue}^{0}}\frac{V_{HA}^{t}}{V_{tissue}^{t}}\\ &=\frac{f_{ef}^{0}}{1-f_{col}^{0}}f_{HA}^{t} \end{aligned} \tag{C.12}$$

with f_{col}^{0} as the initial volume fraction of collagen. Inserting (C.12) into the expression for the extrafibrillar volume fraction (C.6) yields

$$f_{ef}^{t}=\frac{f_{ef}^{0}}{V_{tissue}^{t}/V_{tissue}^{0}}+\frac{f_{ef}^{0}}{1-f_{col}^{0}}\times\left(1-\frac{\rho_{HA}}{\rho_{fl}}\right)f_{HA}^{t} \tag{C.13}$$

Evaluation of (C.13) for $t\to\infty$, and insertion of the corresponding result into extrafibrillar shrinkage expression (C.1) delivers Eq. (11) of Section 2.3.

Appendix D. Derivation of the expression for the fibrillar shrinkage of partially dehydrated tissues, Eq. (17)

In order to downscale (15) to the fibrillar level (where we seek experimental validation through diffraction data), we need to know how the lost fluid volume ΔV_{fl}^{∞} is partitioned between the fibrillar and extrafibrillar spaces, with the respective fractions fulfilling

$$\Delta V_{fl}^{\infty}=\Delta V_{ef,fl}^{\infty}+\Delta V_{fib,fl}^{\infty} \tag{D.1}$$

whereby the overall fluid volume loss can be identified as the dehydration-induced volume loss of the extracollagenous space, ΔV_{ec}^{∞}, and the extrafibrillar volume loss can be identified as the volume loss of the extrafibrillar space:

$$\Delta V_{fl}^{\infty}=\Delta V_{ec}^{\infty}\quad\text{and}\quad\Delta V_{ef,fl}^{\infty}=\Delta V_{ef}^{\infty} \tag{D.2}$$

The evolutions of the extracollagenous and extrafibrillar volumes during dehydration follow from specification of mineral distribution evolution (C.8) for $t\to\infty$ and for vanishing mass formation

rates, $\dot{m}^{\infty}_{HA} = \dot{m}^{\infty}_{ef,HA} = 0$, reading as

$$\frac{\dot{V}_{ec}}{\dot{V}_{ef}} = \frac{\dot{V}_{fl}}{\dot{V}_{ef,fl}} = \frac{m^{\infty}_{HA}}{m^{\infty}_{ef,HA}} \tag{D.3}$$

The mineral mass ratio in (D.3) can be determined as a function of the volume fractions in unmineralized tissue, thanks to Eqs. (C.11) and (C.12)

$$\frac{m^{\infty}_{HA}}{m^{\infty}_{ef,HA}} = \frac{1-f^{0}_{col}}{f^{0}_{ef}} \tag{D.4}$$

with f^{0}_{ef} and f^{0}_{col} according to Eq. (B.5).

Integration of (D.3) from the fully mineralized *and* fully hydrated state, during the entire time span of the (partial or full) dehydration process, results in

$$\frac{\Delta V^{\infty}_{ec}}{\Delta V^{\infty}_{ef}} = \frac{\Delta V^{\infty}_{fl}}{\Delta V^{\infty}_{ef,fl}} = \frac{1-f^{0}_{col}}{f^{0}_{ef}} \tag{D.5}$$

where use of (D.4) was made, and f^{0}_{ef} and f^{0}_{col} still follow from Eq. (B.5). Eq. (D.5), together with (15), (D.1), and (D.2), finally allows for identification of the dehydration-induced fibrillar shrinkage, according to Eq. (17) of Section 2.5.

References

Alexander, B., Daulton, T.L., Genin, G.M., Lipner, J., Pasteris, J.D., Wopenka, B., Thomopoulos., S., 2012. The nanometer-scale physiology of bone: steric modeling and scanning transmission electron microscopy of collagen–mineral structure. J. R. Soc. Interface 9 (73), 1774–1786.

Anderson, H.C., Reynolds, J.J., 1973. Pyrophosphate stimulation of calcium uptake into cultured embryonic bones. Fine structure of matrix vesicles and their role in calcification. Dev. Biol. 34 (2), 211–227.

Anderson, H.C., Garimella, R., Tague., S.E., 2005. The role of matrix vesicles in growth plate development and biomineralization. Front. Biosci. 10, 822–837.

Bala, Y., Farlay, D., Delmas, P.D., Meunier, P.J., Boivin, G., 2010. Time sequence of secondary mineralization and microhardness in cortical and cancellous bone from ewes. Bone 46 (4), 1204–1212.

Baroncelli, GI, Bertelloni, S, Ceccarelli, C, Saggese, G, 1998. Measurement of volumetric bone mineral density accurately determines degree of lumbar undermineralization in children with growth hormone deficiency. J. Clin. Endocrinol. Metab. 83 (9), 3150–3154.

Bertrand, E., Hellmich, C., 2009. Multiscale elasticity of tissue engineering scaffolds with tissue-engineered bone: A continuum micromechanics approach. J. Eng. Mech. 135 (5), 395–412.

Biltz, R., Pellegrino., E., 1969. The chemical anatomy of bone. J. Bone Jt. Surg. 51-A (3), 456–466.

Bohner, M, Baumgart, F, 2004. Theoretical model to determine the effects of geometrical factors on the resorption of calcium phosphate bone substitutes. Biomaterials 25 (17), 3569–3582.

Bonar, L.C., Lees, S., Mook, H.A., 1985. Neutron diffraction studies of collagen in fully mineralized bone. J. Mol. Biol. 181 (2), 265–270.

Brodsky, B., Eikenberry, E.F., Belbruno, K.C., Sterling, K., 1982. Variations in collagen fibril structure in tendons. Biopolymers 21 (5), 935–951.

Burns., C.M., 1929. The effect of the continued ingestion of mineral acid on growth of body and bone and on the composition of bone and of the soft tissues. Biochem. J. 23 (5), 860–867.

Byrne, D.P., Lacroix, D., Planell, J.A., Kelly, D.J., Prendergast, P.J., 2007. Simulation of tissue differentiation in a scaffold as a function of porosity, Young's modulus and dissolution rate: application of mechanobiological models in tissue engineering. Biomaterials 28 (36), 5544–5554.

Colfen., H., 2010. Biomineralization: a crystal-clear view. Nat. Mater. 9, 960–961.

Coussy., O., 1995. Mechanics of Porous Media. John Wiley and sons.

Cuisinier., F.J.G., 1996. Bone mineralization. Curr. Opinion Solid State Mater. Sci. 1 (3), 436–439.

Daymond, M.R., Priesmeyer, H.G., 2002. Elastoplastic deformation of ferritic steel and cementite studied by neutron diffraction and self-consistent modelling. Acta Mater. 50 (6), 1613–1626.

Deakins, M., 1942. Changes in the ash, water, and organic content of pig enamel during calcification. J. Dent. Res. 21, 429–435.

Eanes, E., Lundy, D., Martin, G., 1970. X-ray diffraction study of the mineralization of turkey leg tendon. Calcif. Tissue Int. 6, 239–248.

Fritsch, A., Hellmich., C., 2007. 'Universal' microstructural patterns in cortical and trabecular, extracellular and extravascular bone materials: micromechanics-based prediction of anisotropic elasticity. J. Theor. Biol. 244 (4), 597–620.

Fritsch, A., Hellmich, C., Dormieux, L., 2009. Ductile sliding between mineral crystals followed by rupture of collagen crosslinks: experimentally supported micromechanical explanation of bone strength. J. Theor. Biol. 260 (2), 230–252.

Fritsch, A., Hellmich, C., Dormieux., L., 2010. The role of disc-type crystal shape for micromechanical predictions of elasticity and strength of hydroxyapatite biomaterials. Philos. Trans. R. Soc. A: Math., Phys. Eng. Sci. 368 (1917), 1913–1935.

Gong, J., Arnold, J., Cohn, S.H., 1964. Composition of trabecular and cortical bone. Anat. Rec. 149, 325–332.

Hamed, E., Jasiuk, I., 2012. Elastic modeling of bone at nanostructural level. Mater. Sci. Eng.: R: Reports 73 (3-4), 27–49.

Hammet., F.S., 1925. A biochemical study of bone growth. I Changes in the ash, organics matter and water during growth (mus norvegicus albinus). J. Biol. Chem. 64, 409–428.

Hellmich, C., Ulm, F.-J., 2003. Average hydroxyapatite concentration is uniform in the extracollagenous ultrastructure of mineralized tissues: evidence at the 1–10 μm scale. Biomech. Model. Mechanobiol. 2, 21–36.

Hellmich, C., Barthélémy, J.-F., Dormieux., L., 2004. Mineral-collagen interactions in elasticity of bone ultrastructure – a continuum micromechanics approach. Eur. J. Mech. - A/Solids 23 (5), 783–810.

Hodge, A.J., Petruska, J.A., 1963. Recent studies with the electron microscope on ordered aggregates of the tropocollagen molecule. In: Ramachandran, G.N., (Ed.), Aspects of Protein Structure – Proceedings of the Symposium held in Madras 14–18 January 1963 and organized by the University of Madras, India. Academic Press, London and New York, pp. 289–300.

Jantou, V., Turmaine, M., West, G.D., Horton, M.A., McComb, D.W., 2009. Focused ion beam milling and ultramicrotomy of mineralized ivory dentine for analytical transmission electron microscopy. Micron 40, 495–501.

Jantou-Morris, V., Horton, M.A., McComb., D.W., 2010. The nano-morphological relationships between apatite crystals and collagen fibrils in ivory dentine. Biomaterials 31, 5275–5286.

Katz, EP, Li, S, 1973. Structure and function of bone collagen fibrils. J. Mol. Biol. 80 (1), 1–15.

Lacroix, D., Chateau, A., Ginebra, M.P., Planell, J.A., 2006. Micro-finite element models of bone tissue-engineering scaffolds. Biomaterials 27 (30), 5326–5334.

Lees, S., 1987. Considerations regarding the structure of the mammalian mineralized osteoid from viewpoint of the generalized packing model. Connect. Tissue. Res. 16 (4), 281–303.

Lees, S., 2003. Mineralization of type I collagen. Biophys. J. 85, 204–207.

Lees, S., Heeley, J., 1981. Density of a sample bovine cortical bone matrix and its solid constituent in various media. Calcif. Tissue Int. 33, 499–504.

Lees, S., Mook, H., 1986. Equatorial diffraction spacing as a function of water content in fully mineralized cow bone determined by neutron diffraction. Calcif. Tissue Int. 39, 291–292.

Lees, S., Page., E.A., 1992. A study of some properties of mineralized turkey leg tendon. Connect. Tissue Res. 28 (4), 263–287.

Lees, S., Prostak., K., 1988. The locus of mineral crystallites in bone. Connect. Tissue Res. 18 (1), 41–54.

Lees, S., Heeley, J., Cleary., P., 1979. A study of some properties of a sample of bovine cortical bone using ultrasound. Calcif. Tissue Int. 29, 107–117.

Lees, S., Cleary, P.F., Heeley, J.D., Gariepy, E.L., 1979. Distribution of sonic plesio-velocity in a compact bone sample. J. Acoust. Soc. Am. 66 (3), 641–646.

Lees, S., Bonar, L.C., Mook., H.A., 1984. A study of dense mineralized tissue by neutron diffraction. Int. J. Biol. Macromol. 6 (6), 321–326.

Lees, S, Prostak, KS, Ingle, VK, Kjoller., K, 1994. The loci of mineral in turkey leg tendon as seen by atomic-force microscope and electron-microscopy. Calcif. Tissue Int. 55 (3), 180–189.

Lees, S, Hanson, D., Page, E.A., 1995. Some acoustical properties of the otic bones of a fin whale. J. Acoust. Soc. Am. 99 (4), 2421–2427.

Lees., S., 1981. A mixed packing model for bone collagen. Calcif. Tissue Int. 33, 591–602.

Lemaire, V., Tobin, F.L., Greller, L.D., Cho, C.R., Suva, L.J., 2004. Modeling the interactions between osteoblast and osteoclast activities in bone remodeling. J. Theor. Biol. 229 (3), 293–309.

Lindenmair, A., Wolbank, S., Stadler, G., Meinl, A., Peterbauer-Scherb, A., Eibl, J., Polin, H., Gabriel, C., van Griensven, M., Redl, H., 2010. Osteogenic differentiation of intact human amniotic membrane. Biomaterials 31 (33), 8659–8665.

McNally, E.A., Schwarcz, H.P., Botton, G.A., Arsenault., A.L., 2012. A model for the ultrastructure of bone based on electron microscopy of ion-milled sections. PLoS ONE 7 (1), e29258 01.

Meek, K.M., Fullwood, N.J., Cooke, P.H., Maurice, D.M., Quantock, A.J., Wall, R.S., Worthington, C.R., 1991. Synchrotron X-ray diffraction studies of the cornea, with implications for stromal hydration. Biophys. J. 60 (2), 467–474.

Miles, C., Ghelashvili., M., 1999. Polymer-in-a-box mechanism for the thermal stabilization of collagen molecules in fibers. Biophys. J. 76, 3243–3252.

Morin, C., Hellmich, C., Henits, P., 2013. Fibrillar structure and elasticity of hydrating collagen: A quantitative multiscale approach. J. Theor. Biol. 317, 384–393.

Orlovskii, V.P., Komlev, V.S., Barinov., S.M., 2002. Hydroxyapatite and hydroxyapatite-based ceramics. Inorg. Mater. 38, 973–984.

Orr, J.F, Dunne, N.J, Quinn, J.C, 2003. Shrinkage stresses in bone cement. Biomaterials 24 (17), 2933–2940.

Parfitt., A., 1983. The physiologic and clinical significance of bone histomorphometric data. In: Recker, R. (Ed.), Histomorphometry, Techniques and Interpretation. CRC Press Inc., Boca Raton, USA, pp. 143–223.

Pivonka, P., Zimak, J., Smith, D.W., Gardiner, B.S., Dunstan, C.R., Sims, N.A., Martin, T.J., Mundy, G.R., 2008. Model structure and control of bone remodeling: A theoretical study. Bone 43 (2), 249–263.

Prostak, K.S., Lees, S., 1996. Visualization of crystal-matrix structure. in situ demineralization of mineralized turkey leg tendon and bone. Calcif. Tissue Int. 59, 474–479.
Qin, Q.H., Swain., M.V., 2004. A micro-mechanics model of dentin mechanical properties. Biomaterials 25 (20), 5081–5090.
Rougvie, M.A., Bear., R.S., 1953. An X-Ray diffraction investigation of swelling by collagen. J. Am. Leather Chem. Assoc. 48 (12), 735–751.
Sandino, C., Lacroix., D., 2011. A dynamical study of the mechanical stimuli and tissue differentiation within a CaP scaffold based on micro-CT finite element models. Biomech. Model. Mechanobiol. 10, 565–576.
Sandino, C., Planell, J.A., Lacroix., D., 2008. A finite element study of mechanical stimuli in scaffolds for bone tissue engineering. J. Biomech. 41 (5), 1005–1014.
Scheiner, S., Sinibaldi, R., Pichler, B., Komlev, V., Renghini, C., Vitale-Brovarone, C., Rustichelli, F., Hellmich, C., 2009. Micromechanics of bone tissue-engineering scaffolds, based on resolution error-cleared computer tomography. Biomaterials 30 (12), 2411–2419.
Scheiner, S., Pivonka, P., Hellmich, C., 2013. Coupling systems biology with multi-scale mechanics, for computer simulations of bone remodeling. Comput. Methods Appl. Mech. Eng. 254, 181–196.
Sengers, B.G., Taylor, M., Please, C.P., Oreffo, R.O.C., 2007. Computational modelling of cell spreading and tissue regeneration in porous scaffolds. Biomaterials 28 (10), 1926–1940.
Skinner, H.C.W., Jahren., A.H., 2007. Biomineralization. InTreatise on Geochemistry. Pergamon, pp. 1–69.
Verma, D., Katti, K.S., Katti, D.R., 2010. Osteoblast adhesion, proliferation and growth on polyelectrolyte complex–hydroxyapatite nanocomposites. Philos. Trans. R. Soc. A: Math.., Phys. Eng. Sci. 368 (1917), 2083–2097.
Vuong, J., Hellmich, C., 2011. Bone fibrillogenesis and mineralization: Quantitative analysis and implications for tissue elasticity. J. Theor. Biol. 287, 115–130.
Wergedal, J.E., Baylink, D.J., 1974. Electron-microprobe measurements of bone mineralization rate in-vivo. Am. J. Physiol. 226 (2), 345–352.
Wiesmann, H.P., Meyer, U., Plate, U., Höhling, H.J., 2004. Aspects of collagen mineralization in hard tissue formation. Int. Rev. Cytol. 242, 121–156.
Zylberberg, L., Traub, W., de Buffrenil, V., Allizard, F., Arad, T., Weiner, S., 1998. Rostrum of a toothed whale: ultrastructural study of a very dense bone. Bone 23, 241–247.